



HAL
open science

THERMO-HYDRO FRACTURE AND VISCOELASTIC BEHAVIOR OF TIMBER BASED MATERIALS: NUMERICAL ANALYSIS

Rostand Moutou Pitti, Seif Eddine Hamdi, Frédéric Dubois, Eric Fournely,
Manja Kitek Kuzman

► **To cite this version:**

Rostand Moutou Pitti, Seif Eddine Hamdi, Frédéric Dubois, Eric Fournely, Manja Kitek Kuzman. THERMO-HYDRO FRACTURE AND VISCOELASTIC BEHAVIOR OF TIMBER BASED MATERIALS: NUMERICAL ANALYSIS. WCTE 2016 World Conference on Timber Engineering , Aug 2016, Vienna, Austria. hal-01616937

HAL Id: hal-01616937

<https://hal.science/hal-01616937>

Submitted on 15 Oct 2017

HAL is a multi-disciplinary open access archive for the deposit and dissemination of scientific research documents, whether they are published or not. The documents may come from teaching and research institutions in France or abroad, or from public or private research centers.

L'archive ouverte pluridisciplinaire **HAL**, est destinée au dépôt et à la diffusion de documents scientifiques de niveau recherche, publiés ou non, émanant des établissements d'enseignement et de recherche français ou étrangers, des laboratoires publics ou privés.

THERMO-HYDRO FRACTURE AND VISCOELASTIC BEHAVIOR OF TIMBER BASED MATERIALS: NUMERICAL ANALYSIS

Rostand Moutou Pitti^{1,2,4}, Seif Eddine Hamdi^{1,2}, Frédéric Dubois³, Eric Fournely^{1,2}, Manja Kitek Kuzman⁵

ABSTRACT: The rupture in mixed mode coupling of mechanical and thermal loads for isotropic and orthotropic materials such as wood is studied. The analytical formulation of the energy-release rate is introduced by the integral T and A, which couple the rupture in mixed mode, the thermal effects and the pressure applied on the crack lips. This new formulation is based on the laws of energy conservation and real and virtual mechanical and thermal fields based on the arbitrary, Lagrangian and Eulerian configurations. The Mixed-Mode Crack Growth specimen providing a decrease of the energy-release rate during crack propagation is considered in order to compute the various mixed-mode ratios. The analytical formulation is implemented using the finite-element software Cast3m. The efficiency of the proposed model is justified by showing the evolution of the energy-release rate and the stress-intensity factors versus the crack length and versus the temperature variation in a time-dependent material.

KEYWORDS: mixed mode crack growth, thermal fields, hydric loads, path-independent integral, finite element method, wood material, time-dependent material

1 INTRODUCTION

The micro-cracks commonly occur in many mechanical and civil engineering structures submitted to different loadings [1]. But the main important fact for structural integrity remains the conditions of propagation of these small crack during the lifetime. Combining with mechanical solicitations as fatigue, overload or creep loading, the environmental actions like hydric [2] or temperature [3] play an important role in the propagation of these micro-cracks in the material [4]. In the case of wood, due to its natural origin, its orthotropic and heterogeneous character with different defects such as knots, study these different approaches appear to be essential.

To predict the crack growth process many numerical methods were developed to characterize the mechanical fields around the crack tip. Among them, the background of energy methods come from invariant integrals which enables to evaluate the crack driving forces such as the crack growth rate and the stress intensity factors. The most popular is the J-integral proposed by Rice [5] based on the assessment of the strain energy density and Noether's theorem [6]. This method is inefficient when dealing with mixed mode crack growth problems because it is necessary to separate the displacement field into a symmetric and antisymmetric parts. To circumvent this difficulty, Chen and Shield [7] have developed the M-integral in order to separate fracture modes based on a bilinear form of the strain energy density with virtual mechanical fields [8].

In recent work, a new analytical formulation of A-integral developed by Moutou Pitti et al. [9] and implemented in finite element software by Riahi et al [10] is proposed. This formulation takes into account the effects of thermal load, induced by temperature variation, and complexes boundaries conditions, such as contact between crack lips during crack growth process. However, this approach is limited to stationary crack coupled with a pressure on crack lips and is note suitable to viscoelastic materials and not takes into account the impact of moisture content very essential in wood material.

¹ Rostand Moutou Pitti, Université Blaise Pascal, Istitut Seif Eddine Hamdi, Seif_Eddine.HAMDI@univ-bpclermont.fr

Eric Fournely, Eric.fournely@univ-bpclermont.fr

² CNRS, UMR 6602, IP, F-63171 AUBIERE, France

³ Frédéric Dubois, Université de Limoges, Heterogeneous Material Research Group, Civil Engineering Center, 19300, Egletons, France, frederic.dubois@unilim.fr

⁴ Centre National de la Recherche Scientifique et Technologique (CENAREST), IRT Institut de Recherche Technologique), Libreville, Gabon

⁵ Manja Kitek Kuzman, University of Ljubljana, Biotechnical Faculty, Department of Wood Science and technology, Slovenia, manja.kuzman@bf.uni-lj.si

The first part of this paper presents the material and methods used in this work. The mathematical formulations of the invariant integrals T and A in the case of crack growth process including pressure on crack lips are recalled. Simultaneously, the energy release rate in mixed mode is proposed according to the real and virtual stress intensity factors. Also, the proposed integrals are generalized to viscoelastic materials using a Kelving Voigth model [11] [12] [13]. In the second section, the background of Mixed Mode Crack Growth (MMGC) specimen is proposed [14] [15] [16] [17]. In addition, the numerical routine including the time-dependent increment is described. This specimen is a combination between the Double Cantilever Beam (DCB) [11] and the Compact tension Shear (CTS) specimens [18] and proposes the crack growth stability during the crack tip advanced. The last section is dedicated to study the efficiency of the proposed approach in the case of orthotropic material, where crack growth analysis on wood MMGC specimen is performed with various temperature and internal moisture content for different mixed mode configurations.

2 MATERIAL AND METHODS

2.1 INTEGRAL PARAMETERS IN ELASTIC CASE

In this section we recall the mathematical expression of T and A integrals parameters. According to the conservative and the Noether theorem [6] defined with Arbitrary, Eulerian and langrangian conditions. If we consider a cracked body Ω and Γ a path which surrounds the crack tip oriented by the normal \vec{n} of component n_j , as shown in figure 1, the T -integral is given by (Figure 1) [9]:

$$T = \int_{\Gamma} \frac{1}{2} [\sigma_{ij,k}^v u_i - \sigma_{ij}^u v_{i,k}] n_j d\Gamma + \int_{\Gamma} \frac{1}{2} [\gamma \Delta T_{,j} (v_k - \psi_k) - \gamma \Delta T (v_{k,j} - \psi_{k,j})] n_j d\Gamma - \int_{\Gamma} [\sigma_{ij,k}^v u_{i,j} - \sigma_{ij,k}^u v_{i,j} + \beta \delta_{ij} u_{i,jk} \Delta T] n_j d\Gamma + \int_L \frac{1}{2} [p v_{1,1} - q v_{2,1}] dx_1 \quad (1)$$

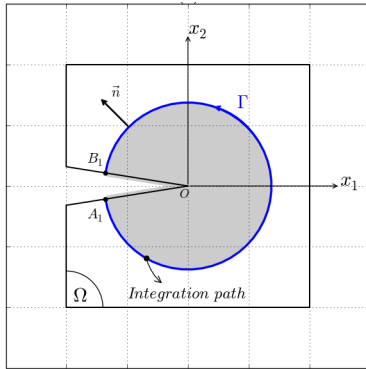


Figure 1: Surface domain integral

In the precedent expression, the first integral is the classical term of the T -integral which represent the effect of mechanical loads applied far from the crack, where σ_{ij}^u and σ_{ij}^v are stress tensor components deduced from

the real displacement field u and the virtual displacement field v , respectively [19]. The second integral represents the effect of thermal load induced by temperature variation ΔT , with ψ is a virtual displacement field as defined by Bui et al [20] and γ is a real coefficient function of material parameters. The third integral represents the pressure crack tip extension during the crack growth process. The last integral represents the effect of pressures p and q applied perpendicularly to the crack lips, where $L = OA_1 + OB_1$ is the integration path, see Figure 2.

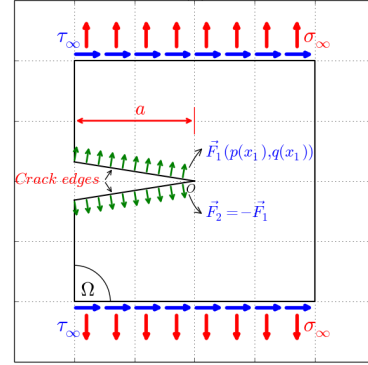


Figure 2: Surface domain integral

Although, experience have shown that integration through curvilinear path induce some inaccuracy on numerical results. To overcome this problem, the curvilinear path is transformed into surface domain by introducing a vector field $\vec{\theta}$ [21] as shown in Figure 3. This mapping function is continuously differentiable and takes these values: $\vec{\theta} = (1,0)$ inside the ring V , and: $\vec{\theta} = (0,0)$ outside it. Hence, the use of the Gauss-Ostrogradsky's theorem enables us to obtain the A -integral given by:

$$A = \int_{\Omega} \frac{1}{2} [\sigma_{ij,k}^v u_i - \sigma_{ij}^u v_{i,k}] \theta_{k,j} dS + \int_{\Omega} \frac{1}{2} [\gamma \Delta T_{,j} (v_k - \psi_k) - \gamma \Delta T (v_{k,j} - \psi_{k,j})] \theta_{k,j} dS - \int_{\Omega} [\sigma_{ij,k}^v u_{i,j} - \sigma_{ij,k}^u v_{i,j} + \beta \delta_{ij} u_{i,jk} \Delta T] \theta_k dS + \int_L \frac{1}{2} F_i v_{i,j} \theta_j dx_1 \quad (2)$$

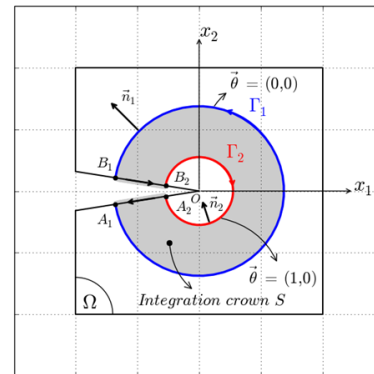


Figure 3: Surface domain integral

2.2 INTEGRAL PARAMETERS IN VISCOELASTIC CASE

2.2.1 Generalized Kelvin Voigt model

The analytical formulation of the A -integral, presented above, is achieved assuming an elastic behavior. Unfortunately, timber has a viscoelastic behavior. In this case, the mechanical fields are time dependent and their computation is not a trivial task. Based on Boltzmann's superposition principle and considering a non-aging linear viscoelastic material, the strain and stress tensors, $\boldsymbol{\varepsilon}$ and $\boldsymbol{\sigma}$ respectively [22] [23]. The generalization to viscoelastic material is introduced by using a generalized Kelvin Voigt model presented in figure 4 [9].

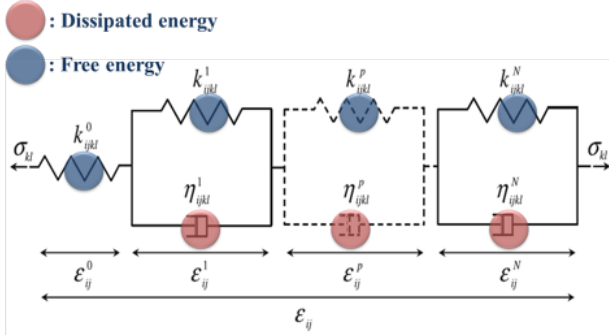


Figure 4: Generalized Kelvin Voigt Model

2.2.2 Viscoelastic integrals parameters

According to the generalized Kelvin Voigt model presented in Figure 4, the expression of integral A (Equation 2) is generalized to viscoelastic behavior as follow:

$$A_v^p = \int_V \frac{1}{2} \left[{}^{(p)}\sigma_{ij,k}^v u_i^{(p)} - {}^{(p)}\sigma_{ij}^u v_{i,k}^{(p)} \right] \theta_{k,j} dV + \int_V \frac{1}{2} \left[\gamma \Delta T_{,j} \delta_{ij} u_{i,jk}^{(p)} \right] \theta_{k,j} dV - \left(\int_V \left[{}^{(p)}\sigma_{ij,k}^v u_{i,j}^{(p)} + {}^{(p)}\sigma_{ij,k}^u v_{i,j}^{(p)} + \beta \delta_{ij} u_{i,jk}^{(p)} \Delta T \right] \theta_k dV \right) + \int_L \frac{1}{2} F_i v_{i,jk}^{(p)} \theta_j dx_1 \quad (3)$$

If $p = (0; 1; \dots; N)$ is the number of Kelvin Voigt cells, the expression (3) becomes:

$$A_v = \sum_{p=0}^N K_v^p \quad (4)$$

According to the expressions, given in Equations (3) and (4), the quantities A_v^p can be computed. The real mechanical fields are then obtained from the response of the p^{th} Kelvin cell to the applied mechanical and thermal (or hydric) loading.

2.3 PHYSICAL INTERPRETATION

Moreover, the A -integral, like M -integral, can be physically interpreted as a particular definition of real stress intensity factors ${}^A K_I^u$ and ${}^A K_{II}^u$. The mixed mode separation can be obtained by performing two distinct computations of ${}^A K_I$ and ${}^A K_{II}^u$ for particular values of ${}^A K_I^v$ and ${}^A K_{II}^v$, such as [9]:

$${}^A K_I^u = 8 \frac{A_v ({}^A K_I^v = 1, {}^A K_{II}^v = 0)}{C_1^p} \quad (5)$$

$${}^A K_{II}^u = 8 \frac{A_v ({}^A K_I^v = 0, {}^A K_{II}^v = 1)}{C_2^p} \quad (6)$$

In equations (5) and (6), C_1^p and C_2^p denote the elastic compliances in opening and shear modes, respectively. The thermal viscoelastic energy release rates in each specific fracture mode ${}^A G_I$ and ${}^A G_{II}$ are finally given by the following expression:

$${}^A G_I = C_1^p \frac{({}^A K_I^u)^2}{8} \quad (3)$$

$${}^A G_{II} = C_2^p \frac{A({}^A K_{II}^v)}{8} \quad (4)$$

2.4 WOOD PROPERTIES

2.4.1 Generalized Kelvin Voigt model

The real wood specimen in Douglas Fir specie is posted in Figure 5 [15].



Figure 5: Wood specimen

The elastic parameters applied in finite element software are summarized bellow

Table 1: Elastic Moduli

Parameters	Values
Longitudinal modulus E_1	15000 MPa
Transverse modulus E_2	600 MPa
Normal modulus E_3	600 MPa
Shear modulus G_{12}	700 MPa
Poisson's coefficient	0.4
Poisson's coefficient	0.4
Poisson's coefficient	0.4

3 MIXED MODE SPECIMEN AND VISCOELASTIC CRACK GROWTH ALGORITHM

3.1 MIXED MODE CRACK GROWTH SPECIMEN

Figure 6 shows the dimensions of wood specimen, with an overall size $210 \times 140 \times 25 \text{ mm}^3$ [15]. The side of the specimen has inclinations with angles of 5° and 10° from the edge and the inferior hill, respectively, as shown in Figure 7. On both hills, four holes were perforated in order to fix the steel Arcans. The distance between the holes centers is 110 mm. The steel Arcans, were performed to allow for mixed-mode configurations. The type of wood used in this test is Douglas and the width of the annual ring varies between 3 and 5 mm and the crack is oriented following the (R/L) direction. An initial crack of 20 mm is machined in the wood specimen in the direction of the fibers.

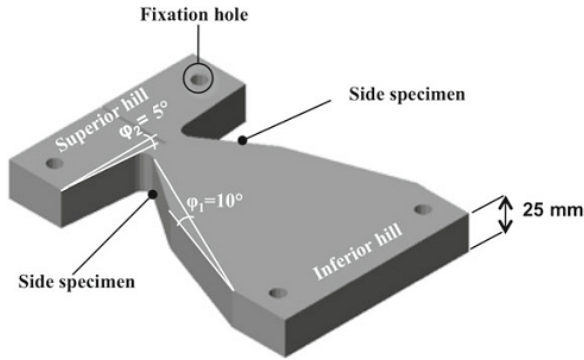


Figure 6: Dimension of wood specimen

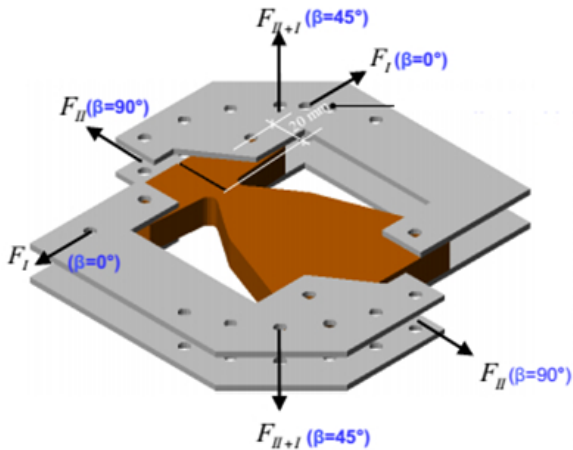


Figure 7: MMGC specimen

The MMGC specimen, shown in Figure 3, is defined by the combination of a modified DCB specimen [11], and CTS specimen [24], on the one hand, and the observation of stability range of energy release rate versus crack length computed numerically with A-method, on the other hand. The main objective of this

specimen is to allow for the decrease in the energy release rate during the tests. The wood specimen, presented in Figure 5, is fixed in a framed structure with Arc-formed handles containing symmetrical holes for load application according to various crack mode ratios β . The application of symmetric loads F_I with angle $\beta = 0^\circ$ is equivalent to the opening mode, and the application of F_{II} , with angle $\beta = 90^\circ$ corresponds to the shear mode as shown in Figure 7. The force F is separated into two forces F_x and F_y corresponding to the axis orientations (x, y) and the mixed-mode ratio in plane configuration. In this work, the mixed-mode fracture tests are obtained by applying the loads F_I and F_{II} with angles $\beta = 45^\circ$.

3.2 NUMERICAL ROUTINE

The analytical formulation of A-integral without taking into account the effect of pressure on the crack lips, was implemented in the finite elements software Cast3m. The MMGC specimen geometry variation versus time (crack evolution) and crack length is considered in the crack growth model. For symmetric geometries and loadings, this crack growth is modelled by moving boundary elements in a semi-mesh. In a mixed mode configuration, this symmetric loading is lost. Then, it is necessary to operate a re-mesh driven by the crack tip advance. In our cases, a fixed crack orientation is supposed. To overcome this difficulty, the hereditary mechanical fields have been projected in the transformed mesh. For a selected temperature, numerical modelling must separate the time and geometry variations. In a first step, all mechanical fields and the crack length a are supposed known at time t_n .

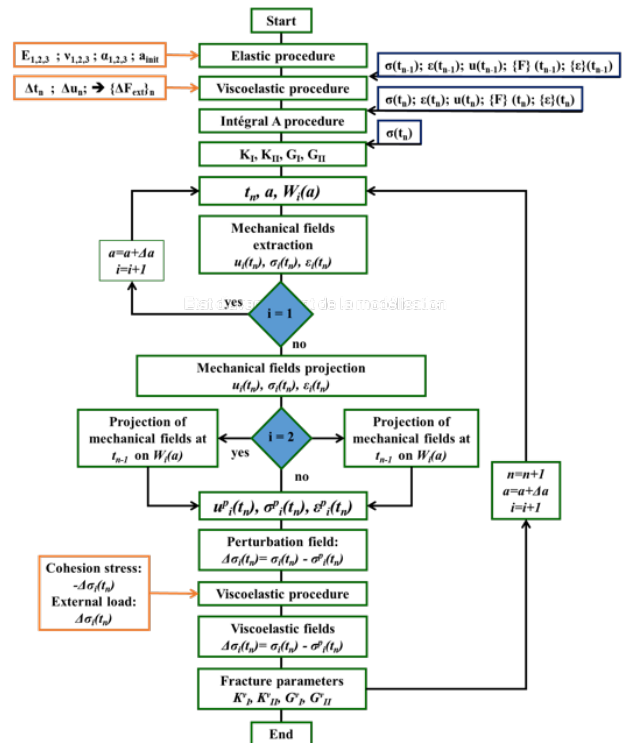


Figure 8: Crack growth routine with thermo-hydro-mechanical fields

Then, stress and external loading, named $\sigma_i(t_n)$ and $F_i(t_n)$, respectively, are defined in the initial mesh noted W_i characterized by a crack length a .

Firstly, the stress perturbation induced by a non-time dependent crack growth is evaluated. The first step consists of considering an instantaneous crack tip advance Δa . New mesh noted W_{i+1} is defined by re-meshing. With the same external loading, an elastic calculation provides the new stress state $\sigma_{i+1}(t_n)$. We note $\sigma(p)_{i+1}(t_n)$ the geometric projection of $\sigma_i(t_n)$ on mesh W_{i+1} . The second step involves calculating, with a differentiation, the stress perturbation $\Delta\sigma_{i+1}$ between the two mesh configurations. The final step involves the application of $-\Delta\sigma_{i+1}$ as a cohesion stress (equivalent external loading) by using the superposition principle. This supplementary loading allows to close the new crack on Δa . In this case, we obtain an equivalent configuration between the first and last steps (same mechanical state and same geometry), but with two different meshes. $\Delta\sigma_{i+1}$ can be interpreted as the stress cohesion in the process zone.

Secondly, the crack length advance is fixed (in our work we fixed $\Delta a = 8$ mm), and time is continuous. Employing the incremental viscoelastic procedure, the stress cohesion $\Delta\sigma_{i+1}$ is employed as an external load vector during the time increment Δt_n . In the time domain, the progressive un-cohesion of crack lips un-cohesion Δa is obtained. The true mechanical state can then be released. Finally, fracture parameters can be computed and the finite elements algorithm is incremented.

4 NUMERICAL RESULTS

4.1 EFFECTS OF THERMAL LOADS

In this last section, we present numerical simulations, which prove the non-path dependence of the A-integral on hereditary behavior and discuss the crack growth process over time. In recent works, Moutou Pitti et al. [13], have shown that this approach is valid for a stationary crack. Now, we propose to generalize the validation by imposing a time dependent crack tip advance according to the numerical procedure presented in section 3. In order to validate A-integral expressions (2), it has been decided to simulate an orthotropic material.

The geometry design is operated by the finite element method. We note that, the numerical analysis is performed under plan stress conditions and based on the finite element mesh depicted in Figure 6 and 7. Moreover, in order to have good accuracy on the computation of the mechanical fields, a refined mesh is adopted in the neighborhood of the crack. In this work, we propose to deal with MMCG specimen with initial crack length ($a = 80$ mm) subjected to tow temperature fields, $T_1 = 20$ °C and $T_2 = 30$ °C, respectively. The numerical meshes of the wood MMCG specimen under the applied temperature fields is shown in Figures 9 and 10.

4.1.1 Numerical meshes

The finite element mesh shown in Figures 9 and 10 in which a circular discretization around the crack tip allows us to define easily the temperature field and the integration crown using parametric elements (θ vector). The MMCG specimen is designed in order to obtain different mixed mode ratios and crack growth stability. The A-integral is performed using virtual finite element displacement fields for opening mode, as an example. The simulations integrate orthotropic viscoelastic behavior for long-term loadings, with elastic moduli given in Table 1.

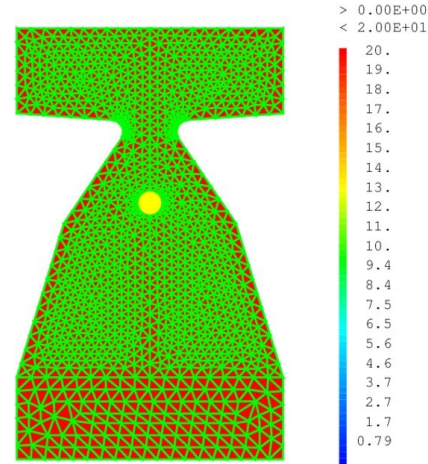


Figure 9: Numerical mesh of the MMCG specimen under temperature field: $T_1=20^\circ\text{C}$.

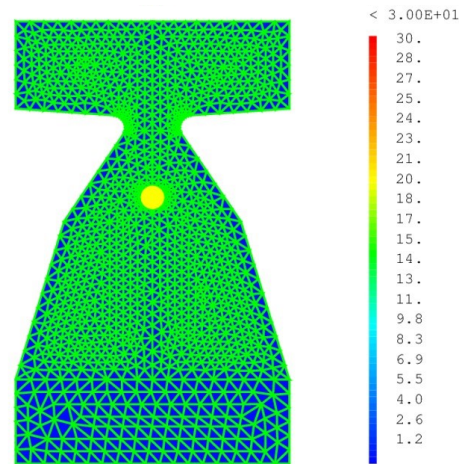


Figure 10: Numerical mesh of the MMCG specimen under temperature field: $T_2=30^\circ\text{C}$.

4.1.2 Energy release rate

For MMCG specimen, Figures 11 and 12 show us the viscoelastic energy release rate evolution versus time and crack growth process for mixed mode using the A-integral concept. The crack growth process can be interpreted as brittle or ductile. If for all cases, the crack growth or damage evolutions in the process zone induce a rigidity decrease, we can note an energy release rate increase during the crack growth advance. With these

considerations, for both mode 1 and mode 2 configurations, we can observe a progressive growing of the process zone (phase of energy release rate increasing) and, in the other hand, a stationary phase with a stabilization of its evolution. More precisely, we can observe, for the first mode G_1 , a greater energy release rate than the second mode G_2 , which correspond on brittle crack tip advance with an approximately peaks values around $8.5 \cdot 10^{-6} \text{ J/m}^2$ for G_1 and $7.8 \cdot 10^{-5} \text{ J/m}^2$ for G_2 . Energy steady state evolution after these peaks illustrate crack growth stabilities for mixed mode calculated with A-integral without taking into account the effect of thermal load induced by a temperature field variation.

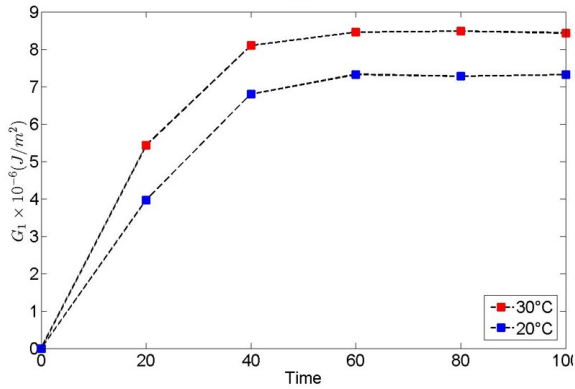


Figure 11: Viscoelastic energy release rate G_1 in mixed mode ($\beta=45^\circ$) versus time under temperature variation ($T_1=20^\circ\text{C}$ and $T_2=30^\circ\text{C}$).

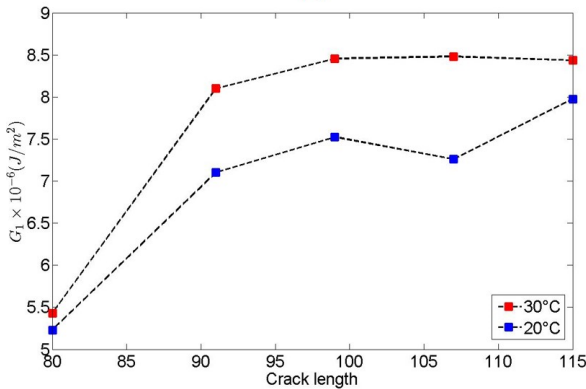


Figure 12: Viscoelastic energy release rate G_1 in mixed mode configuration ($\beta=45^\circ$) during crack growth process ($T_1=20^\circ\text{C}$ and $T_2=30^\circ\text{C}$).

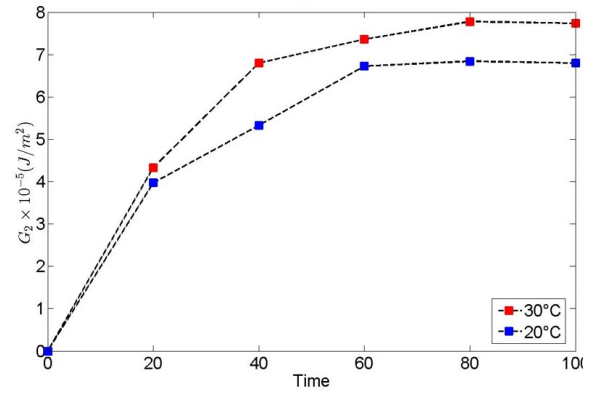


Figure 13: Viscoelastic energy release rate G_2 in mixed mode ($\beta=45^\circ$) versus time under temperature variation ($T_1=20^\circ\text{C}$ and $T_2=30^\circ\text{C}$).

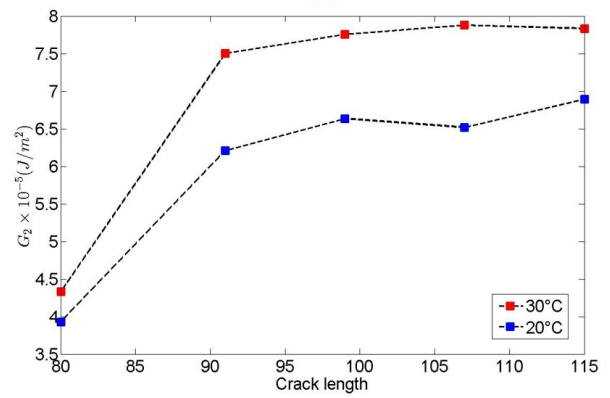


Figure 14: Viscoelastic energy release rate G_2 in mixed mode ($\beta=45^\circ$) during crack growth process under temperature variation ($T_1=20^\circ\text{C}$ and $T_2=30^\circ\text{C}$).

4.2 IMPACT OF THERMO-HYDRO-MECHANICAL LOADING

4.2.1 Numerical meshes

The finite element mesh is shown in Figures 15 and 16 in which a circular discretization around the crack tip allows us to define easily the hydric fields and the integration crown using parametric elements (θ vector).

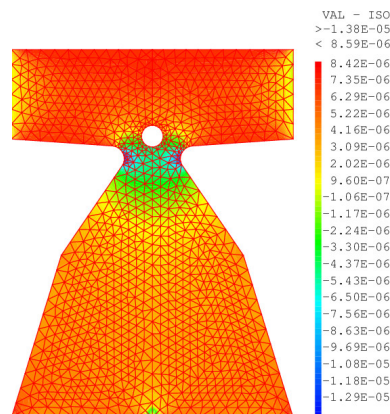


Figure 15: Numerical mesh of the MMCG specimen under temperature field at $T_1=20^\circ\text{C}$.

The MMCG specimen is designed in order to obtain different mixed mode ratios and crack growth stability. The A-integral is performed using virtual finite element displacement fields. In this case, Figures 15 and 16 show the distribution of humidity in a wood specimen according to Exx and Eyy direction respectively.

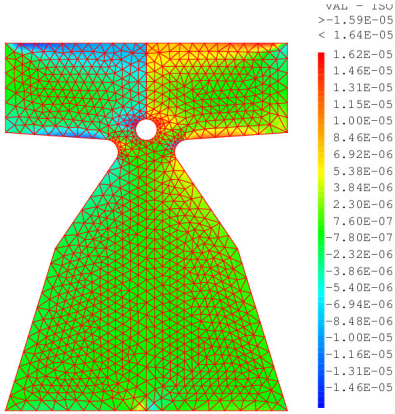


Figure 16: Numerical mesh of the MMCG specimen under temperature field: (a) $T_1=20^\circ\text{C}$. (b) $T_2=30^\circ\text{C}$

4.2.2 Energy release rate

Figure 17 and 18 shows the evolutions of viscoelastic energy release rate in opening mode G_1 and shear mode G_2 respectively, versus time using A_v integral, under a moisture level variation. We note an increase of G with the moisture level. Hence, for both modes, we can observe at first, a progressive increase of G , and then, a stationary phase with a stabilization of its evolution. Specifically, we can observe, for G_2 , a highest energy release rate than G_1 .

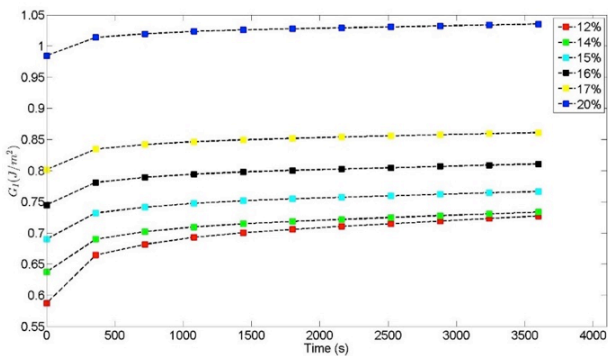


Figure 17: Viscoelastic energy release rate in opening mode

A regular trend in viscoelastic energy levels illustrate the moisture effect stability in mixed mode calculated with the integral A_v without taking into account the effect of thermal expansion induced by a change of the temperature field.

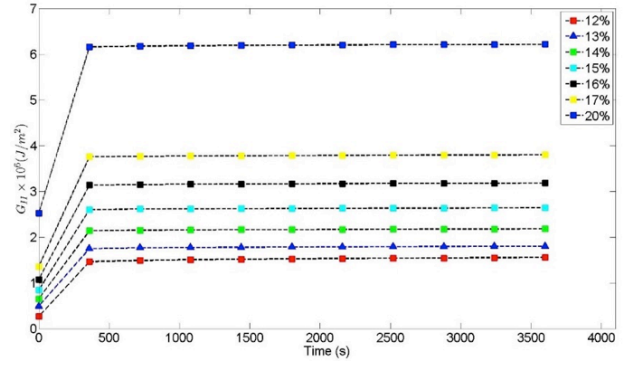


Figure 18: Viscoelastic energy release rate in shear mode.

5 CONCLUSION

The knowledge of crack driving forces such as energy release rate and stress intensity factors is very important in the assessment of the reliability of flawed structures. A new formulation of the A-integral is proposed, which allow to take into account the effect of thermal load induced by temperature variation, without taking into account the mechanical load applied on crack lips. The efficiency of the numerical implementation of crack propagation, in finite element software, is assessed by dealing with orthotropic materials. A good accuracy is observed on the estimates of the viscoelastic energy release rate in mixed mode for both time and crack length evolution. Moreover, the convergence is well achieved since the values of the viscoelastic energy release rate seem to be stabilized throughout the crack path.

In this paper, the analysis is achieved under the assumption of viscoelastic material under static crack propagation and thermo-hydric variation. In addition, the viscoelastic behavior of timber material was implemented in finite element software using spectral decomposition method of the creep tensor. However, automatic crack propagation needs to be achieved accordingly to a critic viscoelastic energy release rate values, which depends on the viscoelastic mechanical properties of timber material. This will be the subject of undergoing researches, in addition to the development of the A-integral in order to take into account the effect of moisture variation. Also, we hope to investigate the effect of uncertainties in the material and load parameters on the reliability of wood structure subjected to crack growth, by using stochastic computation methods. At the end, all numerical results obtained in the present works will be confronted to the experimental data in order to prove the efficiency oh the actual to compute the crack effects in timber structures.

REFERENCES

- [1] Salimi-Majd D., Shahabi F., Mohammadi B. « Effective local stress intensity factor criterion for prediction of crack growth trajectory under mixed mode fracture conditions ». *Theor. Applied Fract. Mech.* (2016) doi.org/10.1016/j.tafmec.2016.01.009
- [2] Moutou Pitti R., Dubois F., Sauvat N., Fournely E. Strain analysis in dried green wood: experimentation and modeling approaches. *Proceedings, 10th Word Conference of Timber Engineering, WCTE, Auckland, New Zeland, July 16-19, 2012.*
- [3] Riahi H., Moutou Pitti R., Dubois F., Fournely E., Chateauneuf A. Numerical fracture analysis coupling thermo-hygro mechanical and viscoelastic behaviour. *Mechanics of Time-dependent Materials (MTDM), Montreal, Canada, 27-30 May, 2014.*
- [4] Hanhijarvi A. « Computational method for predicting the long-term performance of timber beams in variable climates ». *Mater. Struct/Mater. Constr.* 33 (226) (2000) 127-134.
- [5] Rice J.R. A path independent integral and the approximate analysis of strain concentrations by notches and cracks. *J Appl Mech*, 35, 379-386, 1968.
- [6] Noether E. Invariant variations problem. *Transport Theory Stat Phys*, 1, 183-207, 1918.
- [7] Chen F.M.K, Shield R.T. Conservation laws in elasticity of the J-Integral. *J Appl Math Phys*, 28, 1-22, 1977.
- [8] Banks-Sills L., Dolev O. « The conservative M-integral for thermal-elastic problems ». *Int. J. Fract.* 125 (2004) 149–170.
- [9] Moutou Pitti R, Dubois F, Petit Ch. Generalization of T and A integrals to time-dependent materials: analytical formulations. *Int J Fract*, 161, 187-198, 2010.
- [10] Riahi H., Moutou Pitti R., Dubois F., Fournely E. On numerical evaluation of mixed mode crack propagation coupling mechanical and thermal loads in wood material. Vol. 5, 21-26, Springer, 2015.
- [11] Dubois F., Chazal C., Petit C. « Viscoelastic crack growth process in wood timbers: An approach by the finite element method for mode I fracture », *International Journal of Fracture*, Vol. 113, No 4, 2002, pp. 367-388.
- [12] Dubois F., Pop O., Moutou Pitti R., Sauvat N., Petit C., Mario C. An experimental investigation of mixed-mode crack growth process in orthotropic viscoelastic material. *Proceedings, 10th Word Conference of Timber Engineering, WCTE, Osaka, Japan, June 2-5, 2008.*
- [13] Moutou Pitti, R., Dubois, F., Petit, C., Sauvat, N. Mixed mode fracture separation in viscoelastic orthotropic media: numerical and analytical approach by the Mtv-integral. *International Journal of Fracture* 145, 181–193, 2007.
- [14] Moutou Pitti R., Dubois F., Petit C. A new mixed mode fracture specimen (2MCG): numerical and experimental results, *Proceedings, 10th Word Conference of Timber Engineering (WCTE), WCTE, Osaka, Japan, June 2-5, 2008.*
- [15] Moutou Pitti R., Dubois F., Pop O. « On a specimen providing stable mixed mode crack growth in wood material », *Comptes Rendus Mécanique*, Vol. 336, No 6, 2008, pp. 744- 749.
- [16] Moutou Pitti R., Alaa C. Statistical approach and reliability analysis for mixed- mode applied to wood material. *Wood Science and Technology.* 46(6), 1099-1112, 2012.
- [17] Moutou Pitti R., Dubois F., Octavian P. A proposed mixed-mode fracture for wood under creep loadings, *Int J Fract*, 167(2), 195-205, 2011.
- [18] Valentin G., Caumes P. « Crack propagation in mixed mode in wood: a new specimen », *Wood Science and Technology*, Vol. 23, No 1, 1989, pp. 43-53.
- [19] Moutou Pitti R., Dubois F., Petit C., Sauvat N. Fracture of wood under mixed mode loading: numerical approach by the Mv-integral. *Proceedings, 9th Word Conference of Timber Engineering (WCTE), Portland OR, USA, August 6-10, 2006.* [http://www.ewpa.com / wcte/WCTE2006.pdf](http://www.ewpa.com/wcte/WCTE2006.pdf).
- [20] Bui H.D, Proix J.M. Découplage des modes mixtes de rupture en thermoélasticité linéaire par des intégrales indépendantes du contour. *Acte du Troisième Colloque Tendances Actuelles en Calcul de Structure, Bastia, 631-643, 1985.*
- [21] Destuynder Ph, Djaoua M, Lescure S. Some remarks on elastic fracture mechanics. *J de Mécanique Théorique Appliquée*, 2, 113-135, 1983.
- [22] Chateauneuf A., Wassim R., Moutou Pitti R. Reliability of prestressed concrete structures considering creep models. *Structural and Infrastructure Engineering.* pp. 1099-1112, 2013. DOI: 10.1007/s00226-011-0462-7
- [23] Chazal C., Moutou Pitti R. Theoretical and numerical studies of relaxation differential approach in viscoelastic materials using generalized variables. *Journal Theoretical Applied Mechanics.* 50(2), 350-375, 2012.
- [24] Richard HA., Benitz K. « A loading device for the creation of mixed mode in fracture mechanics », *International Journal of Fracture*, Vol. 22, No 2, 1983, pp. R55.